Etienne Braak[1]
Claire Albasi[1,3]
Dominique Anne-Archard[2,3]
Sylvie Schetrite[1]
Marion Alliet[1,3,*]

Impact of Aeration on Mixed Liquor in Submerged-Membrane Bioreactors for Wastewater Treatment

In submerged-membrane bioreactors (SMBRs) for wastewater treatment, aeration with coarse bubbles is applied to limit fouling. The understanding of the different mechanisms between aeration and fouling helps to manage the aeration policy. The impact of aeration (macro scale) on shear stress and mixed-liquor properties (local scale) is evaluated. Experimental characterization of gas-liquid flow in membrane modules, computational fluid dynamics simulation, and controlled breakdown of SMBR mixed-liquor samples are reported. Mean bubble velocities were significantly lower in mixed liquor than in water and the shear stress was one order of magnitude higher in mixed liquor than in water. The floc size decreased and soluble protein concentrations increased with higher shear stress values. Considering the known impacts of these mixed-liquor properties on fouling, the obtained local results explain stronger fouling when coarse bubble aeration increases.

Keywords: Aeration, Computational fluid dynamics, Extracellular polymeric substance, Submerged-membrane bioreactor, Wastewater treatment

DOI: 10.1002/ceat.201600470

1 Introduction

A membrane bioreactor (MBR) is a wastewater treatment device that couples biological treatment and membrane filtration. Membranes achieve physical separation instead of the sedimentation that occurs in the conventional activated sludge process (CASP). This brings important advantages, such as quality and better control of treated water and also intensification of the process, i.e., smaller plant size. Interest in MBRs is growing strongly, both from the research and commercial points of view. However, one of the main drawbacks of the process, which prevents it from spreading wider and faster, is membrane fouling. Aeration near the membrane is most commonly used to limit fouling but it results in high energy consumption, being around 30–50 % of the total energy demand [1, 2].

To decrease this demand and enhance submerged-membrane bioreactor (SMBR) performance, knowledge is required on how the aeration affects fouling. As pointed out by Drews [3], research is often carried out at laboratory scale or with model fluids, so numerical values cannot be transferred to full scale or other plants. Consequently, there is a need to quantify the local phenomena induced by aeration that impact fouling to provide general trends:

- Turbulence can have a positive impact on fouling limitation [4, 5], with particle back transport.
- Wall shear stress at the membrane surface promotes particle removal [6–8].
- But shear stress induced by aeration of the liquid bulk can lead to mixed-liquor breakdown, with a decrease in particle size and release of extracellular polymeric substance (EPS) [9, 10] and can have consequences that are detrimental for filtration performance.

Knowledge regarding purely hydrodynamic mechanisms is growing thanks to computational fluid dynamics (CFD). Wei et al. [11] have drawn up a table of works previously presented in the literature, which can be completed by Tab. 1.

The link between the local phenomena and fouling still needs to be studied although much information is already available: several reviews have tackled the issue of fouling in MBRs [3, 18–20] and the local impact of aeration on fouling, with a focus on hydrodynamics, has been reviewed previously [21].

[1]Dr. Etienne Braak, Dr. Claire Albasi, Sylvie Schetrite, Dr. Marion Alliet
marion.alliet@ensiacet.fr
Université de Toulouse, Laboratoire de Génie Chimique – CNRS-INPT-UPS, 4, Allée Emile Monso, BP 44362, 31030 Toulouse, France.

[2]Dr. Dominique Anne-Archard
Université de Toulouse, Institut de Mécanique des Fluides de Toulouse (IMFT) – CNRS-INPT-UPS, Allée du Professeur Camille Soula, 31400 Toulouse, France.

[3]Dr. Claire Albasi, Dr. Dominique Anne-Archard, Dr. Marion Alliet
Université de Toulouse, Fédération Fermat, c/o Laboratoire de Génie Chimique, 118 route de Narbonne, 31062 Toulouse, France.

Table 1. Summary of CFD modeling and associated experimental work on two-phase flow in various membrane modules since 2013.

Module type	Simulation model	Experiment	Highlight	Ref.
FS MF	3D, VOF, nonuniform grid, mass and momentum equations for each phase	Different bubble sizes (100 mL), Newtonian rheology	Successful simulation of slug bubble in flat-sheet MBR channel. Shear stress in wake region was more intense. Activated sludge viscosity effect found to be minor.	[11]
1. Side stream, 2. HF, 3. hollow sheet, 4. rotational cross flow	RANS, k-ε, diphasic mixture model, calculations with water, recalculation of shear stress using shear rate and power-law model.	Electrochemical shear probes	Four cases of different MBR configurations are studied using CFD. Shear stress increases with higher air flow rate for SMBR. Higher shear stress for rotational MBR (4–11 Pa versus 1–5 Pa with power law rheology). The hollow sheet has a higher power consumption for the same fluid flow rate.	[12]
FS	3D, k-ε turbulent closure equation, two-phase mixed-liquor/air, Euler/Euler. Bingham model for mixed liquor.	200-L Pilot: comparison of the TMP evolution	Fouling model that predicts distributed shear, cake, and flux profiles. Shear distribution profile predicted via multiphase computational fluid dynamics. Model includes dynamic linking of flux and transmembrane pressure. Predicts fouling dynamics with a broad range of scenarios.	[13]
Airlift FS	3D RANS, k-ε turbulent closure equation, two-phase water-air, Euler/Euler	Lab-scale, PIV, water-air,	Baffle location (front, side, or both) and size had significant effects. Side baffles were more effective in elevating membrane surface shear. Maximum shear was obtained with both front and side baffles of optimized size. Role of baffles was more prominent at lower aeration intensities.	[14]
FS	3D RANS, three- phase. Newtonian viscosity function of phase concentration.	Liquid velocity (lapis powder tracer with camera) and gas holdup.	Investigation of the effect of sparger configuration on various hydrodynamic parameters. Higher cross-flow velocity (0.7–1.1 m s^{-1}) between membranes and shear stress on membranes (5–9 Pa) were achieved when the sparger was placed at the bottom of the bioreactor rather than at the entrance of the module.	[15], [16]
HF	Porous media model for the fiber bundle. RANS k-ε; diphasic Euler/Euler; sludge viscosity using Ostwald-de Waele model	PIV and high-speed camera; water-air	Mixed liquor modeled as single phase. Rheological models established for sludge in the absence and presence of iron. Empirical correlations built for fibers with various diameters and packing densities. Fe(II) addition directly to the membrane zone results in higher shear stress.	[17]

FS: flat sheet, HF: hollow fibers, MF: microfiltration, PIV: particle image velocimetry, TMP: transmembrane pressure.

A major gap in knowledge on the relationship between aeration and fouling concerns the link between the impact of aeration and the evolution of the mixed-liquor properties. Many works dealing with fouling and aeration in SMBRs have focused on hydrodynamics and were consequently carried out with simulated suspensions, such as bentonite, latex, baker's yeast, etc., to make the observations easier. This approach has been extended to large MBRs [22, 23], and some generic data and observations have been produced: aeration can have an impact on microbial aggregate properties related to fouling, such as EPS concentrations or floc size, through hydrodynamic shear stress. In their review, Liu and Tay [24] examined the effect of hydrodynamic shear forces in the formation of biofilm and granular sludge. Their conclusions confirm the influence of hydrodynamics on biological properties and the demand for a better understanding of these links.

The results of some studies investigating hydrodynamic conditions in connection with the evolution of EPS concentration combined with fouling of an MBR are summed up in Tab. 2.

As the various conclusions presented above show, no global trend can be deduced from these studies dealing with the link between aeration and mixed-liquor properties. Of course, several reasons can be identified for this situation, and they should help us to set up the main lines of the study. Operational parameter ranges vary from one study to another: first of all, the parameters influencing the biological kinetics, such as the variability of feed composition (real or synthetic) or load often depend on the device used (laboratory or plant scale). Concerning the parameter linked to aeration characterization, it should be noted that some specific aeration demands are rather high compared to those given in the Amedeus project report D1 for a full-scale plant, which are in the range of 0.15–1 $m^3m^{-2}h^{-1}$ (mainly 0.15–0.65 $m^3m^{-2}h^{-1}$) for the specific aeration demand

Table 2. Influence of aeration and/or shear on EPS concentration evolution combined with fouling of MBR.

Module type	Aeration flow rate [$L\,h^{-1}$]	SAD_m [$m^3m^{-2}h^{-1}$]	Shear rate [s^{-1}]	Highlight	Ref.
HF	0–240	0–24		Contribution of solutes and colloids to fouling increased with air flow rate while that of MLSS decreased.	[9]
HF	150, 400, 800	1.5, 4, 8		In the long term (up to 400 h), less fouling obtained by MBR with medium air flow rate, compromise of opposite effects of aeration: cake layer removal and breakage of sludge flocs.	[10]
				Carbohydrate/protein ratio increased with an increase in shear stress	[24]
WWTP sludge			800	Activated sludge flocs with higher carbohydrate/protein ratios are more stable.	[25]
HF	40, 80, 120	0.27, 0.53, 0.8		An increase of aeration implied higher concentration and lower protein/carbohydrate ratio for soluble EPS, both lower concentration and lower ratio for bound EPS, and lower fouling.	[26]
Biofilm MBR		0.84–6.74		Increase of air flow rate with increase of mixed-liquor breakage and of colloidal fraction. Aeration beneficial for filtration, with a plateau region of efficiency for SAD_m above 3.37 $m^3m^{-2}h^{-1}$	[27]
WWTP sludge			1840	In short-term experiments (6 h), high shear rate resulted in an increase of protein concentration.	[28]
FS			160, 1124	In long-term experiments (56 and 134 days), the highest shear rate reduced the concentration of bound and soluble EPS and fouling.	[28]
FS	60	1		Higher shear stress resulted in a thinner, denser, and less permeable biofouling layer, with less heterogeneity and roughness and with more EPS contents.	[29]

FS: flat sheet, HF: hollow fibers, MF: microfiltration, WWTP: wastewater treatment plant.

related to membrane surface (SAD_m)[1] and 10–65 m^3m^{-3} (mainly 10–25 m^3m^{-3}) for the specific aeration demand per unit of permeate produced (SAD_p, equal to the air flow rate per volume of permeate produced). As SMBR configurations differ, the same aeration settings do not induce the same hydrodynamic patterns, or mixed liquor and fouling behavior, highlighting the importance of working at local scale, taking floc size and strength into account.

The work presented here is a first attempt to use a global approach intended to overcome these drawbacks. Its purpose is to establish the influence of operational parameters on local-scale phenomena related to sludge characteristics and their consequences on membrane fouling under operational conditions that are as close as possible to those of industrial plants. This approach requires three main steps, which are further developed:

- Hydrodynamic characterization: experimental determination of bubble velocities and sizes (intermediate-scale parameters) for various air flow rates (macro-scale parameter) in both water and mixed liquor.
- CFD simulations: comparison with experimental results for validation and quantification of shear stress imposed on mixed liquor (local-scale parameter).
- Controlled breakdown of mixed liquor: influence of shear stress on properties of mixed-liquor samples, related to fouling: floc size and soluble EPS concentrations (local-scale parameter).

The global approach is presented in Fig. 1. The parameters studied are on the right-hand side of each frame, the means employed in the method are in bold italics, and the four steps addressed here are noted in the rectangular frames. The methodology is described in more detail in the next section, with reference to papers dealing with technical issues.

Most of the studies published in the literature deal with only one step of this whole approach. Our research focuses on a general approach in the hope of achieving standardization and generalization, which is a recurrent problem cited in reviews dealing with SMBRs and fouling [3, 19–21, 30]. This approach aims to go from a macro parameter, such as air flow rate (operating parameter), to the quantification of local phenomena, e.g., shear stress on the bulk, and their impacts on mixed-liquor properties and fouling.

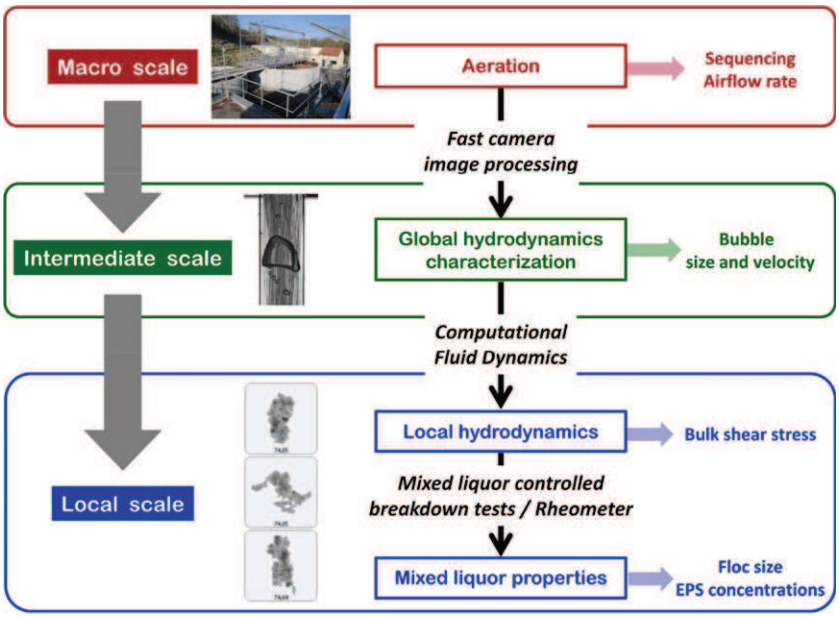

Figure 1. Global approach and steps to link operational parameters to fouling.

2 Materials and Methods

2.1 MBR Devices and Mixed-Liquor Samples

Mixed liquors from two different MBRs were employed. The first one, ML1, was used for tests and validation and came from a full-scale plant in Nailloux, France. The SMBR was fed with domestic wastewater from a treatment plant with a capacity of 4500 P.E. The filtration device was composed of four PURON hollow-fiber modules of 500 m^2 each with a nominal pore size of 0.05 µm. The MBR was operated under continuous membrane aeration, with a sludge retention time of about 100 days and a mixed-liquor suspended solids (MLSS) between 7 and 9 $g\,L^{-1}$. ML1 was taken for the hydrodynamic characterization of air/mixed-liquor flow, where large amounts were needed.

The mixed liquor for the parametric study (ML2) was provided by the laboratory-scale device (15 L) operated in our laboratory in semi external configuration with Polymem modules, using a method close to that described by Lorain et al. [31] with real domestic wastewater, having an MLSS between 8 and 10 $g\,L^{-1}$. The hollow fibers were made of polysulfone and had a nominal pore size of 0.08 µm. The membrane modules had a surface area of 0.225 m^2. The aeration intended to limit fouling was in the range of 75–225 $L\,h^{-1}$, which corresponds to an instantaneous SAD_m range of 0.33–1 $m^3m^{-2}h^{-1}$, close to the range used in full-scale plants. These air flow values served as a basis for hydrodynamic characterization and simulation. The air flow rate was measured and controlled with a Brooks Sho-Rate R2-15-C flowmeter with a Carboloy float. ML2 was employed for controlled breakdown tests, when analysis needed to be done in a short time after the sampling.

Both mixed-liquor samples were characterized rheologically and simulated in CFD (cf. Sect. 2.3.4).

1) List of symbols at the end of the paper.

2.2 Hydrodynamics Characterization

The hydrodynamics was characterized by the bubble size and velocity. Two different modules were used as illustrated in Fig. 2, depending on the fluid studied:

- Observation module: a specific device was built for air/water flow studies in order to obtain a better quality of image. Hollow fibers were replaced by transparent shrink seal tubes (ACLP, France), which enabled a backlight (DEL panel) to enhance the contrast between fibers and bubbles (Fig. 3 a).
- Filtration module: for air/ mixed-liquor flow, the filtration module used in the pilot device enabled the slug velocities to be estimated. The turbidity of the mixed liquor made the interface less clear than in the air/water case. However, as the flow was confined, slugs could be seen between the transparent pipe and the hollow-fiber bundle by transparency (Fig. 3 b). Determination of the interface by a gray level threshold enabled this device to give a reliable estimation of bubble velocity in the mixed liquor.

The observation module was developed in order to obtain properties as close as possible to those of the filtration module. For this, the number of fibers was set to give the same packing density. The characteristics of the two modules are summarized in Tab. 3.

Images were acquired with a fast camera (Motion Blitz Cube 2, Mikrotron), taking up to 500 frames per second with a frame size of 1024×1280 pixels. Images were processed with the image processing program ImageJ. A ruler was used for the conversion from pixel to real size (cm).

First observations showed that the flow pattern was close to slug flow, with mainly large, bullet-shaped bubbles, commonly known as Taylor bubbles (see Figs. 3 a and 3 b), accompanied by some smaller bubbles. This study focused on the Taylor bubbles as they are mainly responsible for the hydrodynamic properties of the flow in confined configurations. They have a higher rising velocity and thus lead to higher shear stress in the surrounding fluid than the small bubbles. The bubble velocity was deduced from the bubble nose positions and the bubble length was estimated from the size of the box bounding the bubble (Fig. 3 c).

In order to allow comparison of our experimental results with those of the literature, care was taken to focus on generic studies. The closest configuration found appeared to be annular flow. Although this comparison may seem to be based on rather broad similarity, the fiber bundle can, in fact, be considered as a full cylinder, i.e., a nonporous and non-moving zone. The first camera observations showed that most of the slugs flowed between the cylindrical pipe and the bundle. Only a few bubbles flowed through the bundle itself, so our assumption was close to physical reality.

Concerning slug flows, three limiting cases have been identified by Wallis [32] for a bubble rising in a stagnant fluid. They are defined from two dimensionless numbers, namely, the Eötvös number and the dimensionless inverse viscosity. An estimation of these numbers allowed it to be sure that the regime studied here experimentally was inertia-dominated, which was confirmed visually by the concave tail shape of the bubble. The surface tension value

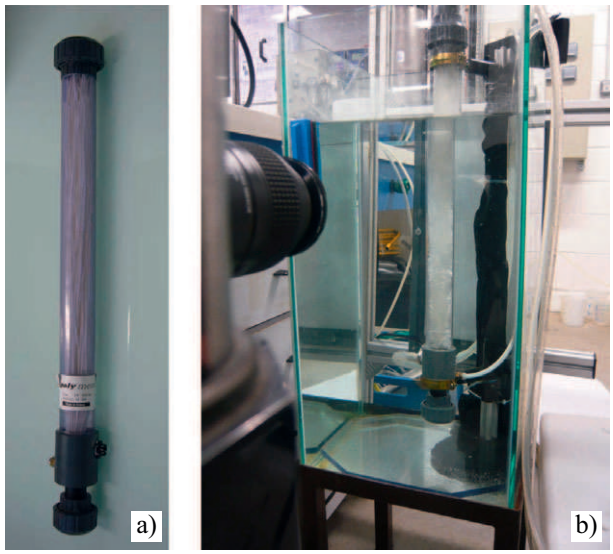

Figure 2. (a) Filtration module with hollow fibers, (b) observation module with transparent shrink seal tubes.

Table 3. Module properties.

Parameter	Filtration module	Observation module
Internal diameter [mm]	37	37
Height [mm]	450	450
External diameter of fibers [mm]	1.45	1.93
Number of fibers	111	68
Membrane surface area [m^2]	0.225	0.185
Packing density [%]	17.04	18.95

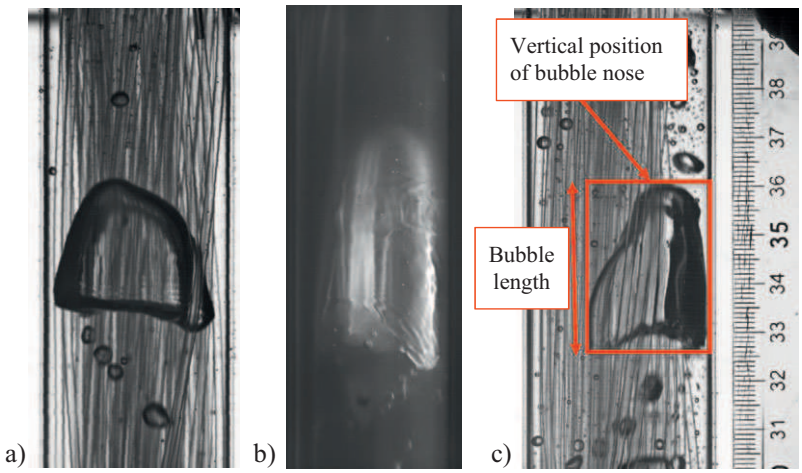

Figure 3. Images of flows: (a) air/water, (b) air/mixed liquor, (c) with estimation of bubble characteristics.

thus had very little influence and water surface tension was used for mixed-liquor simulations.

This flow regime is well-documented for cylindrical tubes [33] and the dimensionless bubble velocity, which is a Froude number, is constant in this case: $U_{rise}/\sqrt{gD} = Fr = 0.35$ where D is the tube diameter and g is the acceleration of gravity. Das et al. [34] extended these results to Taylor bubbles in coaxial cylinders and showed that for air/water flows:

$$U_{rise} = 0.323\sqrt{g(D_{ext} + D_{int})} \quad (1)$$

where D_{int} and D_{ext} are the inner and the outer diameter of the annulus (m), respectively. It is worth noting that the generalization of the Froude number to annular geometries as demonstrated by Das et al. [34] does not involve the hydraulic diameter or the gap, but the quantity (D_{int}+D_{ext}). A comparison of the hydrodynamic conditions used here with those described by Das et al. [34] led to the conclusion that the constant Froude number regime observed by these authors could be applied to the present experiment and thus the rising velocity could be estimated. This gave a value of 0.25 m s^{-1} in the configuration studied, using the fiber bundle diameter as D_{int}. This will be discussed later.

Two distinct cases were considered:

- Single bubble, i.e., the case of one bubble rising in a stagnant fluid. This case was the easier one to treat, experimentally as well as numerically. It was closer to known academic situations and allowed comparison with the previous correlation [34]. This measurement was only performed for air/water flow.
- Slug flow, which constituted a more practical case. In this case, and for a given air flow rate, there was not a single rising velocity, i.e., a velocity identical for all the bubbles, but a distribution of velocities as bubbles influenced each other. Velocities were estimated considering more than 15 bubbles in each case (each flow rate, each liquid).

2.3 Numerical Simulations

2.3.1 Geometry and Meshing

The geometry and the meshes were established with the ANSYS Workbench software, respectively, with Design Modeler and Meshing. Considering the remarks in the previous part, the geometry of the domain was annular and the membrane bundle was simulated as a wall. Some authors have simulated the hollow-fiber bundle as a porous medium [35, 36]. This was not done in our case since it was not necessary for the proposed approach and was time-consuming from the computational point of view. The dimensions were: 0.0125 m inner radius (outer radius of hollow-fiber bundle), 0.0185 m outer radius (inner radius of cylindrical pipe), 0.45 m module height.

Mesh independency was tested as follows. Meshes were retained following a criterion of non-evolution for the bubble rising velocity when the mesh was refined (variance of less than 5 %). As a result, two different meshes were used: an intermediate mesh for air/water simulations and a refined mesh for air/mixed-liquor ones. The main characteristics of the meshes used are described in Tab. 4 (structured meshes).

Table 4. Meshes used.

Element/Meshing	Intermediate	Refined
Membrane & Carter	80	90
Annular space	12	15
Module height	300	350
Number of elements	288 000	472 500

2.3.2 Fluent Parameters

Numerical simulations were carried out with the CFD code ANSYS Fluent 12.1. Given the fact that this work focused on the slugs to characterize the two-phase flow, which led to large air retention values, the volume-of-fluid (VOF) method was selected. As the two-phase flows studied were associated with transitional Reynolds numbers, particularly for air/ mixed-liquor flows, the *Re* normalization group (RNG) k-ε turbulence model that accounts for effects occurring at low *Re* numbers was selected. This choice was confirmed a posteriori by the calculation of a bubble *Re* number (water density $\times U_{rise} \times$bubble equivalent diameter/water viscosity), the maximal value of which is 6000. It has already been used for several CFD simulations related to MBRs [36, 37]. Simulations were performed in transient mode with variation of the time step depending on the Courant number which was set at 0.25. They were carried out on a four-processor PC with a mean computational time of five days.

2.3.3 Simulation Cases

The cases of a single bubble and two bubbles were investigated, considering the second bubble as representative of any bubble in a bubble swarm. This choice was made because (i) in the experiments, the first bubbles were hemispherical, whereas the other bubbles in the swarms were bullet-shaped, so there was a substantial difference between them; (ii) the second simulation bubble described all the velocities of the bubbles of the experimental swarm. This first approximation could be improved in further works.

2.3.3.1 Single Bubble

Simulations were initialized with stagnant liquid. The domain was filled with liquid and an air fraction corresponding to the bubble size and shape was initialized at the bottom of the module. This method did not take phenomena such as bubble formation, coalescence or break-up near the air injection into account. However, it matched reliable Courant numbers ($Co = \frac{\text{velocity} \times \text{time step}}{\text{grid step}} < 1$) with time steps that would lead to convenient simulation times. Simulations were considered as complete when the bubble velocity and its wake were stabilized.

2.3.3.2 Slug Flow

Slug flows were simulated by a periodic cell of two bubbles. These simulations were initialized with the stabilized results of the single-bubble simulation. A second bubble was initialized in its wake without any velocity, using the patch method. The second bubble accelerated in the wake of the first one. The velocities reached by the second bubble swept the velocity range measured in the hydrodynamic characterization for the different air flows tested. On this basis, the second bubble behavior in the simulations run with two bubbles was considered to give a good representation of the flow that occurred in membrane modules and of the shear stress acting on microbial aggregates. The calculation of slug velocity and induced shear stress is detailed in Sect. 2.3.5.

2.3.4 Simulation of Mixed-Liquor Behavior

Most CFD studies are performed considering water as the liquid or simulating mixed liquor as a Newtonian fluid with a constant viscosity depending on the MLSS concentration. The non-Newtonian nature of activated sludge flows [38] is not considered in these cases. The works [13], [17], and [39] should be mentioned as exceptions as they simulate two-phase flows in SMBRs with mixed liquor as a non-Newtonian fluid, using a Bingham [13] and Ostwald-de Waele/power law equation [17, 39].

Following this trend, rheological tests were carried out to determine the best model available in Fluent that matched the mixed-liquor behavior and the parameters required as input for this model. A Mars III rheometer (Thermo Scientific) equipped with serrated plates to avoid slip and a gap of 1.5 mm was used. The protocol comprised two phases: an increase of shear stress from 0.01 to 3 Pa in 240 s and a symmetric decrease. Mixed liquor showed slightly thixotropic behavior which, as a first approach, was not considered in this study. For this reason, only the increasing shear stress region was studied (Fig. 4). The rheological behavior of mixed liquors ML1 and ML2, whatever the sampling date, was viscoplastic, as can be seen in Fig. 4 for results obtained with ML2. The yield stress measured for the various samples ranged from 0.2 to 1.6 Pa. This difference was attributed to differences in nature and MLSS concentrations [38].

Regarding the numerical simulation, the viscoplastic behavior identified for mixed liquors presented a singularity as the viscosity became infinite for zero shear rate. This was overcome by applying regularized models, all of them based on a finite zero-shear-rate viscosity η_0 obtained by clipping the viscosity in the region of very low shear rates without impacting regions having moderate to high shear rates. Among these, the bi-viscosity model and the Papanastasiou model are the best-known but the Carreau model, although defined simply for a shear-thinning fluid, can also be used. This model is defined by the following equation:

$$\eta = \eta_\infty + (\eta_0 - \eta_\infty)\,(1 + (\lambda\dot{\gamma})^2)^{(n-1)/2} \qquad (2)$$

where η_∞, η_0, λ, and n are the infinite shear-rate viscosity (Pa s), the zero shear-rate viscosity (Pa s), the time constant (s), and the flow index, respectively. As long as the flow index is low, typically less than or equal to 0.1, and the ratio η_0/η_∞ is high, this equation is able to represent the drastic increase of the viscosity when the shear rate approaches zero.

Considering the identified viscoplastic behavior, the most convenient rheological model seemed to be the Herschel-Bulkley one. Nonetheless, it did not appear to be the best to model the rheological behavior of the mixed liquor over a large shear rate range. Fig. 4 presents the best fitted curves for ML2 for the Herschel-Bulkley model, the Carreau model, and the power-law model (fit on the range: [0.01 s^{-1}; 350 s^{-1}]).

The power law, although largely used, is clearly not appropriate here. The Carreau model appears to be the most suitable for the sludge studied, particularly for regions of very low and high shear rates, where the fit with experimental points is fairly good. Moreover, as considered here, it is a regularized model, i.e., without infinite viscosity when the shear rate is zero, whereas this still remains to be achieved with the Herschel-Bulkley model. Therefore, the Carreau model was chosen for simulations and the parameters for ML1 and ML2 are presented in Tab. 5.

A higher MLSS led to an increase of the viscosity terms η_∞ and η_0. Nevertheless, the rheological behaviors of both mixed-liquor samples were best fitted by the Carreau model, which exhibited good agreement.

Table 5. Carreau model parameters for mixed-liquor samples.

Mixed-liquor sample	ML1	ML2
MLSS [g L^{-1}]	5.0	8.6
η_0 [Pa s]	5.4	23.2
η_∞ [Pa s]	0.0036	0.0059
λ [s]	49.4	62.7
n	0.10	0.10

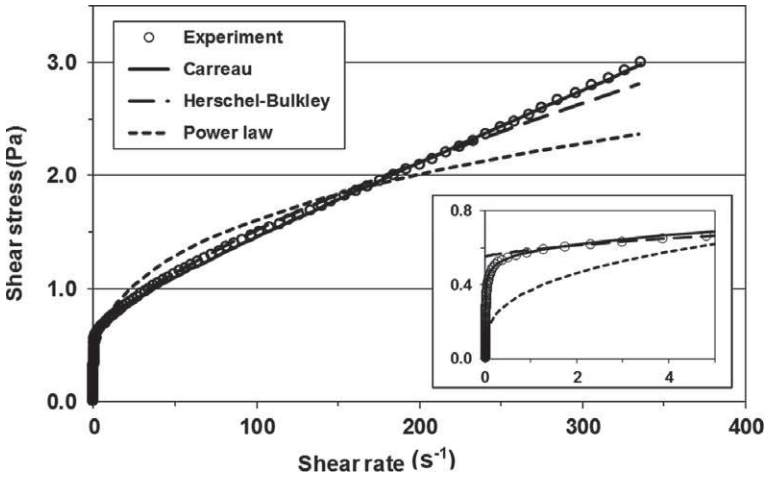

Figure 4. Comparison of rheological models fitted on experimental data.

As explained in Sect. 2.2, the mixed-liquor surface tension and density used for simulations were the values for water, namely, 73 mN m^{-1}, 1000 kg m^{-3}, respectively. Since the flow regime was inertia-dominated, surface tension had very little influence on the results and the variations of density were negligible (0.1 %).

2.3.5 Results and General Considerations

The influence of the shear stress on mixed liquor was analyzed through the stress tensor magnitude $|\tau|$ (Pa). It was calculated from the velocity field V, using the constitutive equation for generalized Newtonian fluids:

$$\underline{\underline{\tau}} = 2\eta(\dot{\gamma})\underline{\underline{D}} \tag{3}$$

where $\underline{\underline{\tau}}$ is the extra-stress tensor, $\underline{\underline{D}} = \frac{1}{2}\left(\nabla V + (\nabla V)^T\right)$ is the strain rate tensor, η is the dynamic viscosity (Pa s), and $\dot{\gamma}$ (s^{-1}) is the magnitude of the rate of strain tensor with $\dot{\gamma} = \sqrt{2\ tr(D^2)}$.

For mean values, the shear stresses were averaged over the wake zone following each bubble. Maximum values were also defined on this zone. Bubble velocities were determined with average values over zones defined using the Fluent isoclip tool with an air-volume fraction above 0.9.

2.4 Sludge Breakdown Tests

To examine the influence of the stress imposed by aeration, samples of mixed liquor were subjected to a shear stress for 225 s, which was the duration of aeration imposed in our pilot SMBR. The imposed shear stresses were in the 0.05–12 Pa range. This was done using an AR 2000 rheometer (TA instruments) equipped with concentric cylinders. The choice to use this rheometer was made because this configuration allowed a larger quantity of mixed liquor to be treated, thus enabling its properties to be measured after shear imposition.

A morphogranulometer (Morphology G3, Malvern instruments SA), which combined microscopy, camera acquisition, and image processing, was employed to estimate the volume mean diameter of the flocs, D[4,3]. To decrease the number of particles for camera acquisition, 1 mL of each mixed-liquor sample was diluted ten times with permeate from the pilot plant, just after shear stress imposition. The protocol relative error measured on three samples was between 2.5 % and 8.5 % depending on the morphological parameter.

The remaining destructured mixed liquor was centrifuged at 4200 *g* just after shear stress imposition to collect the soluble microbial products. Samples were stored at 4 °C. The bicinchoninic acid method [40] was applied to measure the protein concentrations and the anthrone method [41] to determine the carbohydrate concentrations. Measurements were made in triplicate.

The objectives of this intermediate step using a rheometer were to obtain a calibrated shear and to perform the tests with the same mixed liquor. Thus, only the influence of the shear on mixed-liquor properties was considered.

3 Results and Discussion

3.1 Hydrodynamic Characterization

3.1.1 Single Bubble in Water

The first bubble velocity was measured with the observation module for each air flow rate and is presented in Tab. 6.

Table 6. Single-bubble terminal velocity according to air flow rate.

	Air flow rate [L h^{-1}]		
	75	112.5	225
Terminal velocity [m s^{-1}]	0.274	0.303	0.307
Deviation from correlation [%]	+8.7	+20.2	+21.8

As expected, the measured velocities increased with the air flow rate. They were slightly higher than that given by the correlation of Das et al. [34]. These discrepancies may be explained by the design of the air supply device, which induced an increase of water velocity with higher air flow rate, and by the movement of fibers due to bubble impacts. They created forces on the hollow-fiber bundle and could enlarge their pathway. However, because of the relative accuracy of Das' correlation, this study modeled the hollow-fiber bundle as a cylindrical wall. This assumption did not allow hydrodynamics inside the bundle to be characterized but the objective of CFD simulations carried out in this study was to evaluate shear stress in the bulk.

3.1.2 Experimental Comparison of Air/Water and Air/Mixed-Liquor Hydrodynamics

When considering a swarm of bubbles where bubbles influence one another, a velocity distribution appears. Fig. 5 presents this distribution for the three air flow rates tested for both water and mixed liquor. Bubble velocity measurements in the mixed liquor were made with ML1, using the observation module. The evolution of hydrodynamic parameters with air flow rate follows the same trend for air/water and air/ mixed-liquor flows: most cases present a fairly spread distribution centered on mean values, both for water and mixed liquor. These mean values increase with air flow rate, from 0.45 to 0.58 m s^{-1} in water and from 0.33 to 0.43 m s^{-1} in mixed liquor.

A study of two-phase flow hydrodynamics in mixed liquor (8–10 g L^{-1}, the same MLSS range as in the present study) reported on bubble velocities being 15–20 % lower than in water [39]. Although the velocities found in this study are not directly comparable to those of Drews et al. [39] because of the difference of configuration, namely, hollow fiber versus flat sheet, and the fact that different cases are considered, i.e., slug flow versus isolated bubble, a similar trend is observed, with mean velocity values being 18–26 % lower in mixed liquor. This

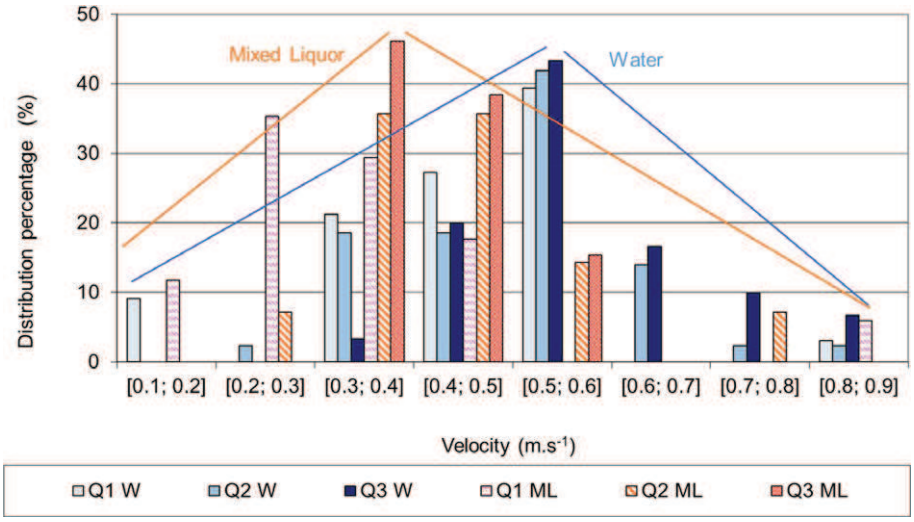

Figure 5. Bubble velocity distributions according to fluid and air flow rates. W: water; ML: mixed liquor; Q1 = 75 L h^{-1}; Q2 = 112.5 L h^{-1}; Q3 = 225 L h^{-1}.

trend has its importance as it validates the CFD simulation in mixed liquor and its good modeling of rheological behavior.

3.2 CFD Simulations

3.2.1 Simulation Validation for Air/Water Flow

The first step of the CFD simulations was a validation for the air/water case, which was carried out by considering the slug velocities. Tab. 7 compares the simulated, experimental, and correlation (provided by Das et al. [34]) velocities for different bubble sizes for air/water flow. The simulation results are in good agreement with the correlation and experimental values, which validates the air/water case.

Table 7. Comparison of simulated, experimental, and correlation [34] velocities for air/water flow.

Bubble length [cm]	Bubble velocity [m s^{-1}]		
	Simulated	Correlation	Experimental
1	0.24	0.25	0.27–0.31
2	0.27	0.25	
3	0.28	0.25	

3.2.2 Simulation Validation for Air/Mixed-Liquor Flow

For the case of a single bubble in mixed liquor, validation was based on the trends observed experimentally for ML1. Using the corresponding parameters (see Tab. 5), in CFD simulations, the mean velocity of a 2-cm bubble was 0.23 m s^{-1} in mixed liquor and 0.27 m s^{-1} in water, i.e., the velocity was 15 % lower in mixed liquor than in water. This corresponds to the trend observed experimentally for slug flow and found by Drews et al. [39] for single bubbles, with rather good agreement. It confirms, firstly, that the viscosity has an important effect on this flow and, secondly, that modeling mixed liquor with a fluid corresponding to the Carreau model rheology is a suitable assumption.

3.2.3 Simulation Results

The general pattern of two-phase flow is that the fluid rises on the bubble side and comes downstream on the opposite side. This pattern could be assimilated to an airlift cell in the bubble's zone of influence. A second remark that can be made regarding the qualitative analysis is that the zone of influence of the bubble is smaller in mixed liquor than in water, for both the wake and the recirculation region as illustrated in Fig. 6.

These observations were made for single bubbles, as the results were clearer and simpler to interpret without bubble interactions. The trend was the same when two bubbles were considered for slug-flow simulation.

The latter case is more interesting from a quantitative point of view, as it is more representative of real flow in membrane modules. The acceleration of the second bubble initialized in the stabilized wake of a first bubble enabled to scan almost the entire velocity range observed experimentally in the previous part (Fig. 5). Both mean and maximum values of the shear stress were determined on a volume that included the bubble and its wake for each bubble.

The global trend was for mean and maximum values to increase with bubble size and velocity. Given that greater bubble size and velocity were observed at higher air flow rate, increasing the aeration, in the studied range, may have led to higher stress on the bulk and potentially to a greater breakdown of the mixed liquor.

The comparison between air/water and air/mixed-liquor also provided some interesting information. Tab. 8 summarizes the shear stress values according to bubble velocity in the two fluids for a 5 cm long slug initialized in the wake of a 2 cm long bubble.

Table 8. Mean and maximum values of shear stresses according to bubble velocity for a 5-cm long slug and fluid.

Water			Mixed-liquor 2		
Bubble velocity [m s^{-1}]	Shear stress [Pa]		Bubble velocity [m s^{-1}]	Shear stress [Pa]	
	Mean	Max.		Mean	Max.
0.37	0.07	1.20	0.28	0.98	8.86
0.45	0.09	1.31	0.40	1.05	6.88
0.51	0.11	1.35	0.46	1.09	9.75
0.62	0.16	1.65	0.56	1.14	11.1

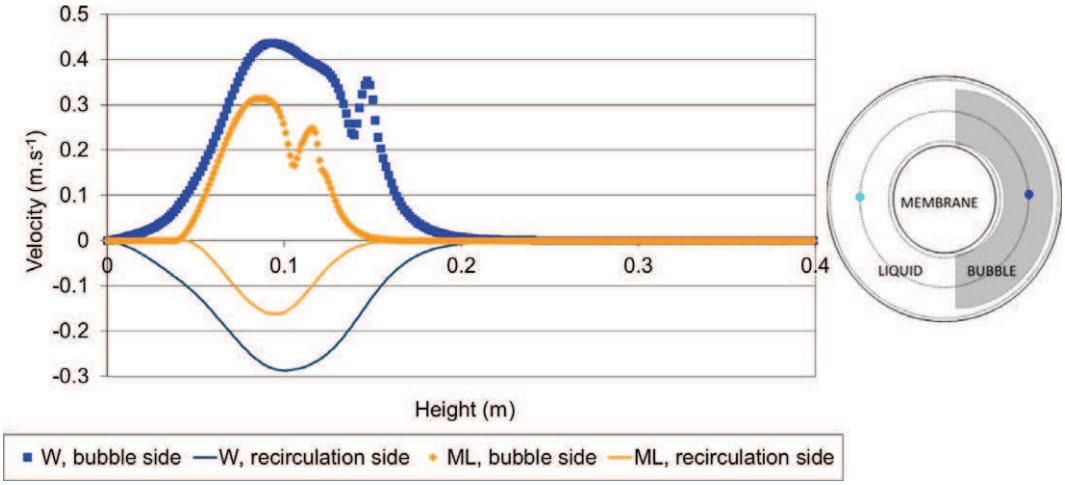

Figure 6. Velocity profiles for a 2-cm long slug on bubble and recirculation sides; W: water, ML: mixed liquor. Positions of the profiles in a top view of the membrane module.

It is noticeable that the maximum shear stress values found for air/water flows in this study are close to those found in the literature. CFD simulations have been reported for two-phase flow modeling in tubular [37] and flat sheet [15, 42, 43] membranes, which estimate wall shear stress. These simulations provide maximum values in the 0.7–4 Pa range for air/water flows. Similarly, Martinelli et al. [44] found a maximal value of 0.25 Pa for air/water flow in a hollow-fiber configuration. Our simulations are in good agreement with these values, which indicates that the results presented are reliable, thus allowing to moving forward to the next simulation phase.

It is of particular interest to deduce from Tab. 8 that the shear stresses were one order of magnitude higher in mixed liquor than in water, with values of around 1 Pa in mixed liquor against 0.1 Pa in water for mean values, and around 10 Pa in mixed liquor against 1 Pa in water for maximum values.

For comparison:

- Wei et al. [11], who used a Newtonian model for viscosity, found the maximum value of shear stress of around 5 Pa at the membrane wall for very large bubbles, the influence of this rheology being small.
- Ratkovich and Bentzen [12], who used a power law model to recalculate shear stress from a water/air simulation, found shear stresses of between 2 and 5 Pa for the SMBR case.
- Amini et al. [15], who used a viscosity function of the distribution of the solid, found a maximum mixed-liquor shear stress of around 9 Pa.
- Liu et al. [17], who applied an Ostwald-de Waele model for the viscosity and considered small bubbles, found a shear stress lower than 2 Pa.
- In an experimental work, Böhm and Kraum [45] measured the shear stresses caused by a xanthan solution, following an Ostwald-de Waele shear-thinning rheological approach, on a flat sheet membrane using an electrodiffusion method. They found shear stress median values of 3.2 Pa and maximum values of up to 9.1 Pa.

This observation has consequences regarding practical issues. The estimation of maximum wall shear stress is not the same for mixed liquor and water. Although air/water simulations are necessary for the fundamental understanding of the phenomena involved in the process performance, this difference highlights the importance of taking the rheological behavior of mixed liquor into account in order to estimate the flow properties and provide values transposable to full-scale plants. The size of the bubbles seems to have quite an important influence on shear stresses, with coarse bubbles giving higher shear stress values. The values obtained for ML2 served as a basis for comparison in controlled breakdown tests.

3.3 Controlled Breakdown of Biological Media

The results of controlled breakdown tests are presented in Fig. 7 with the evolution of the floc $D[4,3]$ and of the soluble EPS concentrations versus shear stress.

The yield stress measured for the ML2 sample considered was 1.6 Pa and stressing with this value corresponded to the maximum floc $D[4,3]$ value. For higher shear stresses, the floc $D[4,3]$ decreased. It should be noted that the floc $D[4,3]$ was also lower for shear stress below the yield value, i.e., 0.1 and 1.1 Pa, for which the shear rate was theoretically zero, and was measured to be around $10^{-4}\,s^{-1}$ in practice. The fact that the flow first promoted particle aggregation and then led to floc breakdown when it became too high could account for these results. From the yield value of 1.6 Pa to the maximum shear stress imposed of 10 Pa, the floc $D[4,3]$ decreased from 157 to 92 µm. For comparison, a strength and breakage study of activated sludge floc from a WWTP showed a destructuring shear stress around 3 Pa [46].

Soluble protein concentrations increased with shear stress, from 20–25 mg L^{-1} below the yield stress to 46 mg L^{-1} at 10 Pa. Carbohydrate concentrations remained almost constant, with values around 30–35 mg L^{-1}. This trend is very close to that observed by Menniti et al. [28], with a release of protein under higher shear applied in the short term but no release of carbohydrates, correlated with higher fouling in their study.

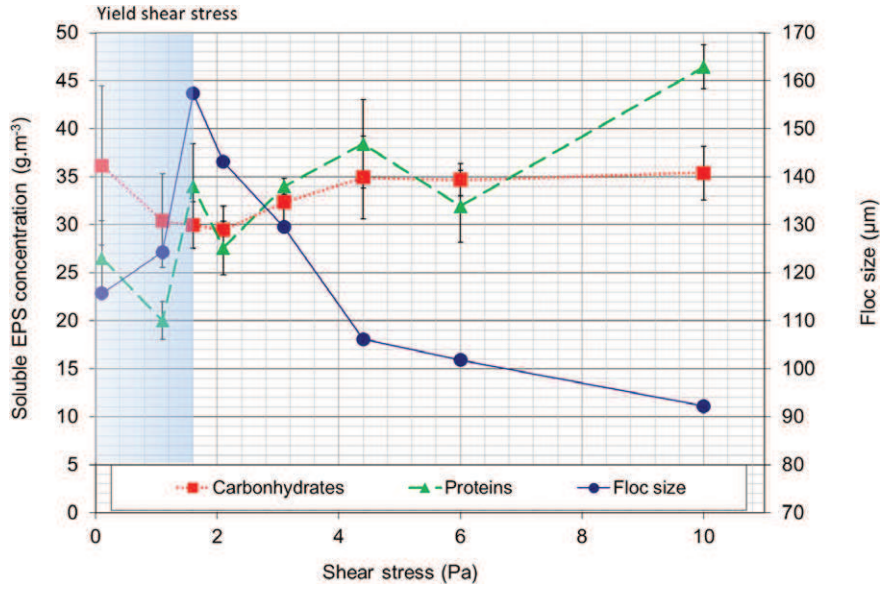

Figure 7. Evolution of floc $D[4,3]$ and soluble EPS concentrations with shear stress.

An impact of shear stress on mixed-liquor properties, particularly floc $D[4,3]$ and soluble protein concentrations, was highlighted by these tests in a range of shear stress values from 1.5 to 10 Pa. This range corresponds to stresses between the mean and maximum value evaluated by CFD simulations. Thus, aeration imposed on an industrial range of parameters (SAD_m) may lead to mixed-liquor breakdown in the short term.

4 Conclusions

This study has aimed to bridge the gap between macro and local scale by establishing relationships between the operating parameter (air flow rate), the hydrodynamics at macroscopic scale (slug bubble sizes and velocities observed experimentally with a fast camera), the hydrodynamics at local scale (shear stress on mixed-liquor bulk estimated numerically), and the properties of the biological medium (floc size and soluble EPS). Important insights have been gained on all the issues tackled:

- The simulation of mixed-liquor samples from SMBRs as Carreau fluids was a convenient assumption.
- Differences in hydrodynamics between air/water and air/mixed-liquor flows were highlighted. (i) Experimentally: slug velocity was 18–26 % lower in mixed liquor than in water in the air flow rate range tested. (ii) Quantification of shear stresses on the bulk showed that they were one order of magnitude higher in mixed liquor, namely, around 1 and 10 Pa, respectively, for mean and maximum values, than in water with around 0.1 and 1 Pa, respectively, for mean and maximum values.
- Controlled breakdown of mixed-liquor samples showed that an increase of shear stress induced a floc $D[4,3]$ decrease and, to a lesser extent, an increase of protein in soluble EPS. These shear stresses corresponded to those estimated numerically for the air flow rate imposed on our pilot plant, which was close to the range of aeration parameters used in full-scale plants.

Although coarse bubble aeration is a good method for limiting fouling on SMBRs, a too high flow rate not only implies higher costs but may also have a detrimental effect on fouling because of floc breakage. A local impact of the increase of aeration flow rate was demonstrated. The bulk shear stress produced may rise to the range that modifies the mixed-liquor properties in a sense that is known to have a negative impact on fouling: decrease of floc size, increase of protein concentration. If these results are confirmed with a full-scale design, it would then be convenient to determine the threshold by a simple rheological test and characterize the minimum air flow depending on the bundle design.

Further work is required to verify this study at full scale, to fully define the relationship with fouling and to quantify the importance of biological local mechanisms compared with the other local mechanisms like turbulence and wall shear stress.

The authors have declared no conflict of interest.

Symbols used

Co	[–]	Courant number
$\underline{\underline{D}}$	[–]	strain rate tensor, $\frac{1}{2}\left(\nabla V + (\nabla V)^T\right)$
$D[4,3]$	[m]	volume mean diameter of the flocs
D_{int}, D_{ext}	[m]	inner and outer diameter of an annulus
Fr	[–]	Froude number
g	[m s^{-2}]	acceleration due to gravity, 9.81
n	[–]	flow index
SAD_m	[m^{3}m^{-2}h^{-1}]	specific aeration demand related to membrane surface
SAD_p	[–]	specific aeration demand related to permeate volume
U_{rise}	[m s^{-1}]	rising velocity
V	[m s^{-1}]	velocity field

Greek letters

$\dot{\gamma}$	[s^{-1}]	magnitude of the rate of strain tensor, $\sqrt{2\,tr(D^2)}$
λ	[s]	time constant
η	[Pa s]	dynamic viscosity
η_∞	[Pa s]	infinite shear-rate viscosity
η_0	[Pa s]	zero shear-rate viscosity
$\underline{\underline{\tau}}$	[–]	extra-stress tensor

Abbreviations

CFD	computational fluid dynamics
EPS	extracellular polymeric substances
MBR	membrane bioreactor
ML	mixed liquor
ML1, ML2	mixed liquor 1 and 2
MLSS	mixed-liquor suspended solids
SMBR	submerged membrane bioreactor
W	water
WWTP	wastewater treatment plant

References

[1] S. Judd, *Trends Biotechnol.* **2008**, *26 (2)*, 109–116. DOI: 10.1016/j.tibtech.2007.11.005

[2] J. A. Gil, L. Túa, B. Montaño, M. Rodríguez, D. Prats, *Desalination* **2010**, *250 (3)*, 997–1001. DOI: 10.1016/j.desal.2009.09.089

[3] A. Drews, *J. Membr. Sci.* **2010**, *363 (1–2)*, 1–28. DOI: 10.1016/j.memsci.2010.06.046

[4] T. Ueda, K. Hata, Y. Kikuoka, O. Seino, *Water Res.* **1997**, *31 (3)*, 489–494. DOI: 10.1016/S0043-1354(96)00292-8

[5] A. P. S. Yeo, A. W. K. Law, A. G. Fane, *J. Membr. Sci.* **2006**, *280 (1–2)*, 969–982. DOI: 10.1016/j.memsci.2006.03.029

[6] G. Ducom, F. P. Puech, C. Cabassud, *Desalination* **2002**, *145 (1–3)*, 97–102. DOI: 10.1016/S0376-7388(02)00044-3

[7] C. Gaucher, P. Legentilhomme, P. Jaouen, J. Comiti, J. Pruvost, *Exp. Fluids* **2002**, *32 (3)*, 283–293. DOI: 10.1007/s003480100317

[8] P. R. Bérubé, G. Afonso, F. Taghipour, C. C. V. Chan, *J. Membr. Sci.* **2006**, *279 (1–2)*, 495–505. DOI: 10.1016/j.memsci.2005.12.043

[9] F. Fan, H. Zhou, *Environ. Sci. Technol.* **2007**, *41 (7)*, 2523–2528. DOI: 10.1021/es062035q

[10] F. Meng, F. Yang, B. Shi, H. Zhang, *Sep. Purif. Technol.* **2008**, *59 (1)*, 91–100. DOI: 10.1016/j.seppur.2007.05.040

[11] P. Wei, K. Zhang, W. Gao, L. Kong, R. Field, *J. Membr. Sci.* **2013**, *445*, 15–24. DOI: 10.1016/j.memsci.2013.05.036

[12] N. Ratkovich, T. R. Bentzen, *Water Sci. Technol.* **2013**, *68 (12)*, 2534–2544. DOI: 10.2166/wst.2013.515

[13] A. Boyle-Gotla, P. D. Jensen, S. D. Yap, M. Pidou, Y. Wang, D. J. Batstone, *J. Membr. Sci.* **2014**, *467*, 153–161. DOI: 10.1016/j.memsci.2014.05.028

[14] X. Yan, K. Xiao, S. Liang, T. Lei, P. Liang, T. Xue, K. Yu, J. Guan, X. Huang, *Bioresour. Technol.* **2015**, *175*, 633–637. DOI: 10.1016/j.biortech.2014.10.133

[15] E. Amini, M. R. Mehrnia, S. M. Mousavi, H. Azami, N. Mostoufi, *RSC Adv.* **2015**, *127*, 105218–105226. DOI: 10.1039/C5RA18727C

[16] E. Amini, M. R. Mehrnia, S. M. Mousavi, H. Azami, N. Mostoufi, *Ind. Eng. Chem. Res.* **2013**, *52 (29)*, 9930–9939. DOI: 10.1021/ie400632y

[17] X. Liu, Y. Wang, T. D. Waite, G. Leslie, *Water Res.* **2015**, *75*, 131–145. DOI: 10.1016/j.watres.2015.02.009

[18] F. Meng, S.-R. Chae, A. Drews, M. Kraume, H.-S. Shin, F. Yang, *Water Res.* **2009**, *43 (6)*, 1489–1512. DOI: 10.1016/j.watres.2008.12.044

[19] P. Le-Clech, V. Chen, T. A. G. Fane, *J. Membr. Sci.* **2006**, *284 (1–2)*, 17–53. DOI: 10.1016/j.memsci.2006.08.019

[20] F. Meng, S. Zhang, Y. Oh, Z. Zhou, H.-S. Shin, S.-R. Chae, *Water Res.* **2017**, *114*, 151–180. DOI: 10.1016/j.watres.2017.02.006

[21] E. Braak, M. Alliet, S. Schetrite, C. Albasi, *J. Membr. Sci.* **2011**, *379 (1–2)*, 1–18. DOI: 10.1016/j.memsci.2011.06.004

[22] B. Verrecht, C. James, E. Germain, W. Ma, S. Judd, *Water Sci. Technol.* **2011**, *63 (6)*, 1217–1223. DOI: 10.2166/wst.2011.361

[23] R. Van den Broeck, P. Krzeminski, J. Van Dierdonck, G. Gins, M. Lousada-Ferreira, J. F. M. Van Impe, J. H. J. M. van der Graaf, I. Y. Smets, J. B. van Lier, *J. Membr. Sci.* **2011**, *378 (1–2)*, 330–338. DOI: 10.1016/j.memsci.2011.05.010

[24] Y. Liu, J. H. Tay, *Water Res.* **2002**, *36 (7)*, 1653–1665. DOI: 10.1016/S0043-1354(01)00379-7

[25] G. P. Sheng, H. Q. Yu, X. Y. Li, *Biotechnol. Bioeng.* **2006**, *93 (6)*, 1095–1102. DOI: 10.1002/bit.20819

[26] L. Ji, J. Zhou, *J. Membr. Sci.* **2006**, *276 (1–2)*, 168–177. DOI: 10.1016/j.memsci.2005.09.045

[27] I. Ivanovic, T. O. Leiknes, *Desalination* **2008**, *231*, 182–190. DOI: 10.1016/j.desal.2007.11.046

[28] A. Menniti, S. Kang, M. Elimelech, E. Morgenroth, *Water Res.* **2009**, *43 (17)*, 4305–4315. DOI: 10.1016/j.watres.2009.06.052

[29] A. Ding, H. Liang, G. Li, N. Derlon, I. Szivak, E. Morgenroth, W. Pronk, *J. Membr. Sci.* **2016**, *510*, 382–390. DOI: 10.1016/j.memsci.2016.03.025

[30] W. Naessens, T. Maere, I. Nopens, *Bioresour. Technol.* **2012**, *122*, 95–106. DOI: 10.1016/j.biortech.2012.05.070

[31] O. Lorain, P. E. Dufaye, W. Bosq, J. M. Espenan, *Desalination* **2010**, *250 (2)*, 639–643. DOI: 10.1016/j.desal.2009.09.040

[32] G. B. Wallis, *One-Dimensional Two-Phase Flow*, McGraw-Hill, New York **1969**.

[33] M. Ramdin, R. Henkes, *J. Fluids Eng.* **2012**, *134*, 41303–41311. DOI: 10.1115/1.4006405

[34] G. Das, P. K. Das, N. K. Purohit, A. K. Mitra, *Chem. Eng. Sci.* **1998**, *53 (5)*, 977–993. DOI: 10.1016/S0009-2509(97)00210-8

[35] Y. Wang, M. Brannock, S. Cox, G. Leslie, *J. Membr. Sci.* **2010**, *363 (1–2)*, 57–66. DOI: 10.1016/j.memsci.2010.07.008

[36] S. Buetehorn, D. Volmering, K. Vossenkaul, T. Wintgens, M. Wessling, T. Melin, *J. Membr. Sci.* **2011**, *384 (1–2)*, 184–197. DOI: 10.1016/j.memsci.2011.09.022

[37] N. Ratkovich, C. C. V. Chan, P. R. Berube, I. Nopens, *Chem. Eng. Sci.* **2009**, *64 (16)*, 3576–3584. DOI: 10.1016/j.ces.2009.04.048

[38] I. Seyssiecq, J. H. Ferrasse, N. Roche, *Biochem. Eng. J.* **2003**, *16 (1)*, 41–56. DOI: 10.1016/S1369-703X(03)00021-4

[39] A. Drews, H. Prieske, E. L. Meyer, G. Senger, M. Kraume, *Desalination* **2010**, *250 (3)*, 1083–1086. DOI: 10.1016/j.desal.2009.09.113

[40] P. K. Smith, R. I. Krohn, G. T. Hermanson, A. K. Mallia, F. H. Gartner, M. D. Provenzano, E. K. Fujimoto, N. M. Goeke, B. J. Olson, D. C. Klein, *Anal. Biochem.* **1985**, *150 (1)*, 76–85. DOI: 10.1016/0003-2697(85)90442-7

[41] J. Weiner, *J. Inst. Brew.* **1978**, *84 (4)*, 222–223. DOI: 10.1002/j.2050-0416.1978.tb03876.x

[42] N. V. Ndinisa, A. G. Fane, D. E. Wiley, *Sep. Sci. Technol.* **2006**, *41 (7)*, 1383–1409. DOI: 10.1080/01496390600633873
[43] H. Prieske, L. Böhm, A. Drews, M. Kraume, *Desalin. Water Treat.* **2010**, *18 (1–3)*, 270–276. DOI: 10.5004/dwt.2010.1784
[44] L. Martinelli, C. Guigui, A. Line, *Desalination* **2010**, *250 (2)*, 587–591. DOI: 10.1016/j.desal.2009.09.029
[45] L. Böhm, M. Kraume, *J. Membr. Sci.* **2015**, *475*, 533–544. DOI: 10.1016/j.memsci.2014.11.003
[46] Y. Yuan, R. R. Farnood, *Powder Technol.* **2010**, *199 (2)*, 111–119. DOI: 10.1016/j.powtec.2009.11.021